NUCL SCI TECH (2018) 29:25
https://doi.org/10.1007/s41365-018-0365-5

Evaluation of interfacial properties in SiC composites using an improved cohesive element method

Hang Zang[1] · Xing-Qing Cao[1] · Chao-Hui He[1] · Zhi-Sheng Huang[1] · Yong-Hong Li[1]

Received: 29 December 2016 / Revised: 15 May 2017 / Accepted: 21 May 2017 / Published online: 5 February 2018

Abstract A two-dimensional axisymmetric finite element model based on an improved cohesive element method was developed to simulate interfacial debonding, sliding friction, and residual thermal stresses in SiC composites during single-fiber push-out tests to extract the interfacial bond strength and frictional stress. The numerical load–displacement curves agree well with experimental curves, indicating that this cohesive element method can be used for calculating the interfacial properties of SiC composites. The simulation results show that cracks are most likely to occur at the ends of the experimental sample, where the maximum shear stress is observed and that the interfacial shear strength and constant sliding friction stress decrease with an increase in temperature. Moreover, the load required to cause complete interfacial failure increases with the increase in critical shear strength, and the composite materials with higher fiber volume fractions have higher bearing capacities. In addition, the initial failure load increases with an increase in interphase thickness.

Keywords Fiber push-out test · Cohesive element model · SiC composites · Finite element method · Interfacial properties

This work was supported by the National Natural Science Foundation of China (No. 11405124), Science Challenge Project (No. TZ2018004), Natural Science Basic Research Plan in Shaanxi Province of China (No. 2015JQ1030), and the Shaanxi Province Postdoctoral Science Foundation (2014).

✉ Hang Zang
zanghang@xjtu.edu.cn

[1] School of Nuclear Science and Technology, Xi'an Jiaotong University, Xi'an 710049, China

1 Introduction

SiC composites are candidate materials for use in certain fusion reactor designs because of their inherent high-temperature properties and low activation under high-energy neutron irradiation [1, 2]. An essential issue determining the successful application of such composites is the fiber/matrix interfacial behavior, because composites transfer stresses between the fiber and the matrix via the interface [3]. Different indirect methods such as fragmentation testing, pull-out testing, and push-out testing have been developed to determine the interfacial properties (e.g., interfacial bond strength and roughness) of composites. Among these techniques, the single-fiber push-out test is regarded as the most important because the procedures for sample preparation and testing are relatively simple. However, only the average interfacial shear strength and sliding friction stress can be obtained from push-out testing, and fiber fracture causes problems during loading or in the case of indenter failure in the experiment [4]. Therefore, it is necessary to analyze the fiber push-out process using analytical or numerical methods in order to achieve a better understanding of the interfacial behaviors and to interpret the experimental results of fiber push-out tests.

In the past decade, different analytical methods based on the variational model [5, 6] and shear-lag theory [7–9] have been developed to convert the load–displacement data from push-out experiments to interfacial properties. However, these methods usually entail simple assumptions. For example, the shear-lag assumes that load is transferred from an infinite matrix to an infinitely long fiber in the shear direction; hence, the obtained results are approximate values. Recently, some finite element models have been developed to study the interfacial behaviors of composites during push-out tests. Dinter et al. [10] analyzed the distribution of interfacial stresses in the case of complete bonding and sliding. Ananth et al. [11] and Honda et al. [12] performed analyses of interfacial debonding with various shear strength criteria. Some researchers adopted the energy failure criterion to calculate the interfacial fracture energy of various SiC composites [13–15]. Zeng et al. [16] conducted single-fiber push-out experiments on SiC/Ti composites in the temperature range from 20 to 530 °C and then developed a finite element model based on the spring element method to quantitatively evaluate the interfacial shear strength and sliding friction coefficient. Geubelle and Baylor [17] developed a cohesive element theory considering sliding friction as a subroutine to analyze the interfacial behaviors of graphite/epoxy laminates. Lin et al. [18] applied this cohesive element theory to a polyester/epoxy system. You et al. [19] defined a traction–separation law that included the equivalent frictional stress for the cohesive element to study Cu-matrix composites.

Among the finite element models analyzing the interfacial failure of composites during push-out tests of the interphase layer model [20, 21], spring element model [4, 13, 22, 23], and cohesive element model [3, 18, 24], the interphase model defines a layer with a specified physical thickness and material properties. However, it cannot be used to describe interfacial failure. In the spring method based on fracture mechanics, stress easily occurs at crack tips. The cohesive element method is convenient relative to the others; the cohesive elements close to zero thickness are embedded in the interface, while the cohesive damage region is embedded at crack tips where the failure criterion is satisfied. The parameters of this cohesive element without physical meaning are identified based on fitting values from push-out experiments. Generally, the cohesive element with a bilinear or exponential constitutive law was used to simulate failure occurring normal to the interface [25]. To analyze the tangential failure of the interface, the constitutive law has been appropriately improved.

To analyze the interfacial behaviors of SiC composites during push-out tests, a two-dimensional axisymmetric finite element model based on an improved cohesive element method is presented here. In this analysis, firstly, the validity of this improved cohesive element for simulating interfacial debonding and sliding friction is confirmed. Second, the importance of temperature is discussed; residual thermal stresses are introduced into composites from the stress-free temperature to the test temperature by the mismatch of thermal expansion coefficients between the fiber and the matrix materials. Finally, the effects of the interfacial shear strength, fiber volume fraction, and interphase thickness on the interfacial behaviors of SiC composites are investigated.

2 Finite element analyses

2.1 Improved cohesive element constitution equation

The interphase layer is a chemical reaction-produced layer between the fiber and the matrix. Hence, the interphase layer is usually very thin, and cohesion is actually the internal force in the interphase layer from atom–molecule interactions. The cohesive element model, simplified in this case, can reflect the mechanical behaviors of the reaction product layer when the appropriate parameters are selected.

The cohesive element obeys the defined traction–separation law, as shown in Fig. 1, which assumes initially linear elastic behavior, followed by the initiation and evolution of damage (complete failure at u_f). The relation between strain and displacement u is shown below:

$$\varepsilon = \frac{u}{t}, \tag{1}$$

where u is the relative displacement of the two contacting element faces attached to a cohesive element and t is the constitutive thickness of the cohesive elements.

Usually, the traction–separation law is expressed in terms of displacement instead of strain. The initial linear elastic constitutive equation is shown below:

$$\sigma = Kt = (E/t)u, \tag{2}$$

where E and K denote the modulus and stiffness, respectively, and σ is the stress.

Several initiation criteria and evolution laws are available in the ABAQUS modeling software [25]. Because the

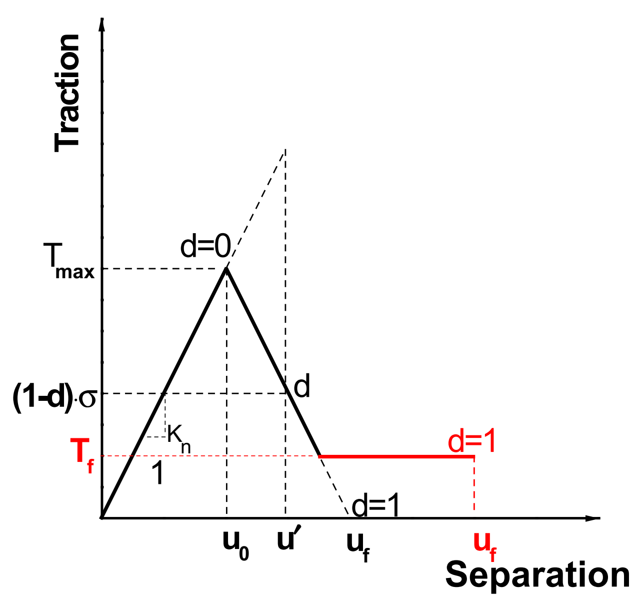

Fig. 1 Improved traction–separation law

main failure mechanism during push-out testing of SiC composites is shear stress failure of the interface, the maximum shear stress failure criterion is used in this study:

$$|\tau| \geq T_{\max} = \tau^* + \tau_{\mathrm{f}}, \tag{3}$$

where τ^* and τ_{f} denote the critical shear strength and sliding frictional stress, respectively, and $T_{\max}$ is the maximum shear stress. The cohesive element begins to fail when the shear stress reaches $T_{\max}$.

The damage evolution is based on the $1 - d$ reduction of the stiffness, where d is the damage variable. The stress σ^{f} of the failure of cohesive elements is expressed as follows:

$$\sigma^{\mathrm{f}} = (1-d)K\mathrm{u} = (1-d)\sigma. \tag{4}$$

To ensure that the shear stress declines to the constant value T_{f}, equal to the sliding frictional stress, after the failure, the damage variable d is given as

$$d = 1 - \frac{c}{u_0 + u'}, \quad u = u_0 + u', \tag{5}$$

$$\sigma^{\mathrm{f}} = cK_n = T_{\mathrm{f}}, \tag{6}$$

where u_0 and u' denote the initial and relative failure displacements, respectively, and c is a fitting constant. The damage variable as a function of the displacement is achieved through tabulation.

2.2 Modeling the fiber push-out test

The 2D axisymmetric finite element model shown Fig. 2 was proposed to simulate the single-fiber push-out test. In order to compare the experimental results with those reported by Zeng et al. [16], SiC/Ti-matrix composites were chosen to build the model. The model defines four zones: (1) the SiC fiber; (2) the cohesive zone; (3) the Ti matrix; and (4) the average material surrounding the matrix, having effective composite properties calculated from the linear rule of mixtures. In this analysis, the SiC fibers and Ti matrix are regarded as perfectly isotropic elastic materials, while the average material is treated as a

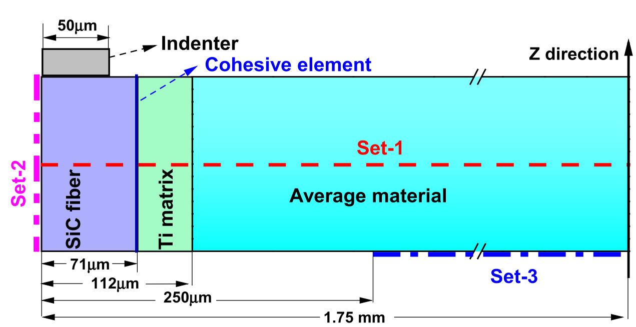

Fig. 2 (Color online) Finite element model of single-fiber push-out test for SiC/Ti composite

transverse isotropic elastic material. The slice height is 0.43 mm, SiC fiber radius is 71 μm (including an 18-μm-thick carbon core and a 3-μm-thick pyrolytic carbon protection layer), Ti matrix radius is 112 μm with a fiber volume fraction equal to 40%, and the outer radius of the composite slice is 1.75 mm. The radii of the indenter and the constraint boundary are 50 and 250 μm, respectively. The single-fiber push-out test model is established at 20, 300 and 530 °C, using the material data given in Ref. [16]. The stress-free temperature is assumed to be 770 °C, which is the sample preparation temperature.

The finite element analysis was performed using ABAQUS. The elements of the fiber, matrix, and average material are CAX4 (four-node bilinear axisymmetric quadrilaterals); the elements of the cohesive zone are COHAX4 (four-node axisymmetric cohesive elements); and the elements of the indenter are RAX2 (two-node linear axisymmetric rigid links). Zero-thickness cohesive elements are embedded between the fiber and matrix elements. The chosen element size (including the cohesive element) is 6.32 μm in the z-direction. The fiber push-out analysis involves the following steps.

First, the sample is cooled from the stress-free temperature to the testing temperature; then, residual thermal stresses are introduced by the mismatch of thermal expansion coefficients between SiC and Ti. In this analysis, the cooling process is modeled by temperature loading from the initial temperature of 770 °C. The boundary conditions on Set 1 and Set 2 in this step are described as

$$U_z^{\mathrm{f}}(r, h/2) = U_z^{\mathrm{m}}(r, h/2) = U_z^{\mathrm{ave}}(r, h/2) = 0, \tag{7}$$

$$U_{\mathrm{r}}(0, z) = 0, \tag{8}$$

where U_z^{f}, U_z^{m}, and U_z^{ave} represent the axial displacements of the fiber, matrix, and average material, respectively; U_{r} represents the radial displacement; and h is the sample thickness. In addition, the free-end face of the specimen can be realized by removing the existing tying constraint. According to Ref. [22], an initial crack (length: 6.32 μm) is introduced at both ends of the specimen to realize the free-end face of the specimen; this initial crack length is far smaller than the SiC fiber radius and its addition does not affect the peak load.

The second step is the loading of a small displacement to establish stable contact between the rigid indenter and the fiber. The indenter is square instead of pyramidal to avoid stress concentration, and the contact is modeled as frictionless to improve the convergence; otherwise, the contact iteration solution could be disconcerted divergence by a sudden large load. The boundary condition on Set 3 in this step is described as

$$U_z(r, 0) = 0 \quad (250\,\mu\mathrm{m} \leq r \leq R^{\mathrm{ave}}), \tag{9}$$

where R^{ave} is the outer radius of the average material.

The third step is the modeling of the fiber push-out process. Fiber push-out is simulated with the displacement-controlled loading of a single fiber until this fiber is pushed out completely from the matrix. The cohesive elements start to fail when the shear stress reaches the maximum shear stress during the fiber push-out test; this means that the crack grows before the shear stress reaches a constant value, similar to the sliding frictional stress.

2.3 Verification of the improved cohesive element method

2.3.1 *Damage evolution law and traction–separation relation*

Since the failure mechanism is mainly shear failure, as mentioned earlier, only the shear damage evolution law is discussed here, although cases of both normal and shear damages are considered. The previously described damage evolution law is plotted in Fig. 3a. The cohesive element does not fail before the initial failure displacement u_0, at which the shear stress is equal to the maximum shear stress and the damage variable d always remains equal to zero. The sudden increase in d as it rapidly approaches 0.9 indicates the beginning of failure, meaning that debonding occurs, since d then increases very slowly from 0.9 to 1 (final failure).

The relationship between the traction and the separation distance of the cohesive element is shown in Fig. 3b. In the early stage of separation, the traction increases linearly with the separation distance. When the shear stress reaches the critical value, the interface falls off, and the traction drops to a constant value related to the temperature. Usually, the solution of this drastic change is difficult to converge. In this study, viscous regularization is introduced to improve the convergence.

2.3.2 *Verification process*

Fiber push-out tests were simulated using this improved cohesive element method. The validity of the method for simulating interfacial debonding and sliding friction should be confirmed, and the effects of some geometry and physical parameters on the mechanical behaviors of the composites were investigated. Figure 4a exhibits the experimental load–displacement curve of the push-out test of the SiC/Ti composites at 20 °C from Ref. [16]. The relation between load and displacement is nearly linear for loads below the maximum load P_{max}. P_i is approximately 17 N according to the displacement of the fiber protruding from the bottom of the slice after complete (instable) debonding. According to Ref. [11], the linear relation remains because of the very slow crack expansion. The interface debonds fully at P_{max}. Hereafter, the load decreases to the sliding frictional force from the existence of interfacial roughness.

Under the critical shear strength τ^* of 500 MPa and the constant frictional stress T_f of 84 MPa, the simulated load–displacement curves with various indenter radii at 20 °C are shown in Fig. 4b. From the comparison of the experimental and computational curves, the simulated maximum load and frictional force show good agreement with the experimental values, and the P_i value of 15 N is similar to that in the experiment (17 N). As shown in Fig. 4b, the simulated value is lower than the experimental value in Fig. 4a, and the displacement increases with decreasing indenter radius R. The difference may be related to the

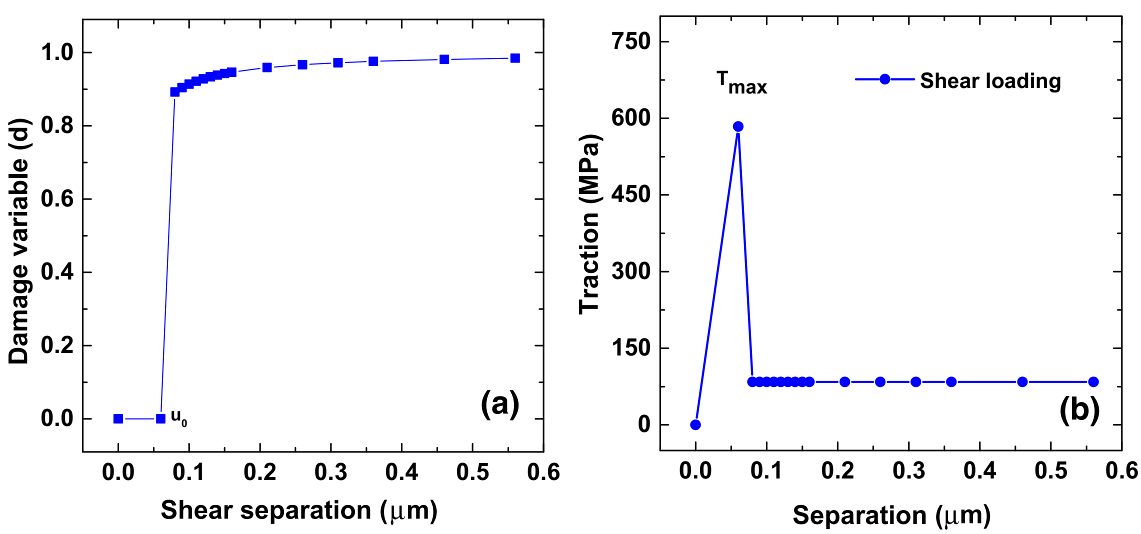

Fig. 3 (Color online) Variation of damage variable (**a**) and traction (**b**) with separation distance at 20 °C

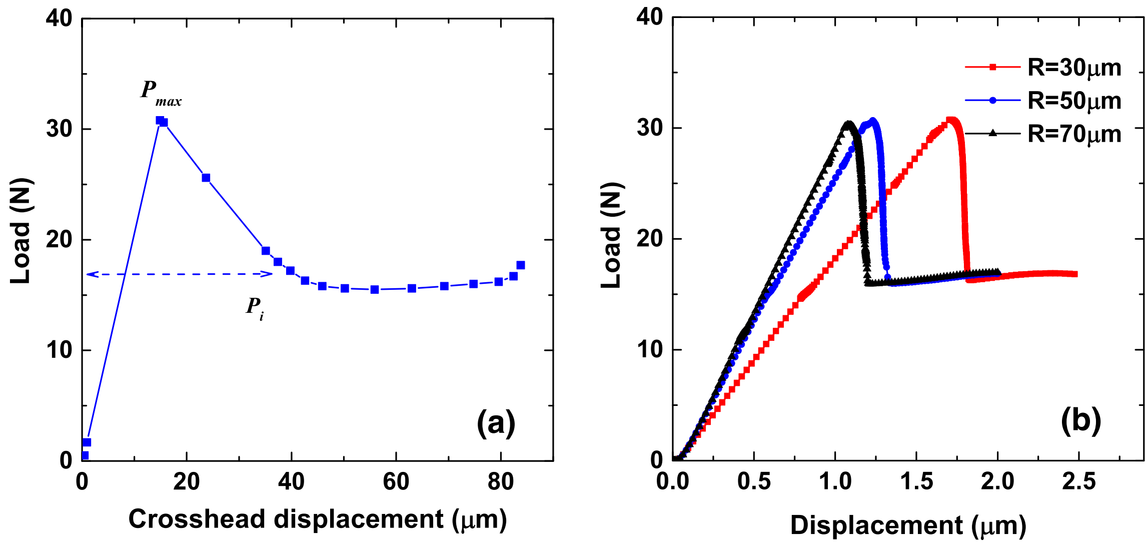

Fig. 4 (Color online) The experimental and computational Load–displacement curves at RT, which (**a**) is the push-out test [16] and **b** is the simulation under different indenter radii

shape selection of the indenter; in order to facilitate convergence, a square indenter is used in the simulation instead of the triangular indenter in the experiment.

Figure 5a describes the corresponding distribution of shear stress from the bottom to the top of the interface. It clearly demonstrates that the shear stress introduced by loading is negative; as a result, the bottom residual shear stress is larger and the top shear stress is smaller. The bottom of the interface starts to fail when the load reaches the initial failure load of 15 N; then, as the load increases, the cracks propagate from the bottom to the top. However, the propagation direction of the cracks relates to the height of the sample. According to Ananth et al. [11], a critical height of $\sim$ 0.5–0.75 mm is observed in SiC/Ti composites; the crack propagates from the top to the bottom along the interface when the sample height exceeds this critical height.

As mentioned earlier, the viscous coefficient is introduced to resolve the severe nonlinearity of the cohesive element after failure. Viscous regularization is discussed in detail in Ref. [25]. The variations in external work, total energy, internal energy, and viscous energy over time are shown in Fig. 5b. Note that the time is calibrated by the analysis steps. The total energy increases from zero to 0.02 mJ only during the cooling stage as thermal energy converts to internal energy; the external work only increases during the fiber push-out. This means that the

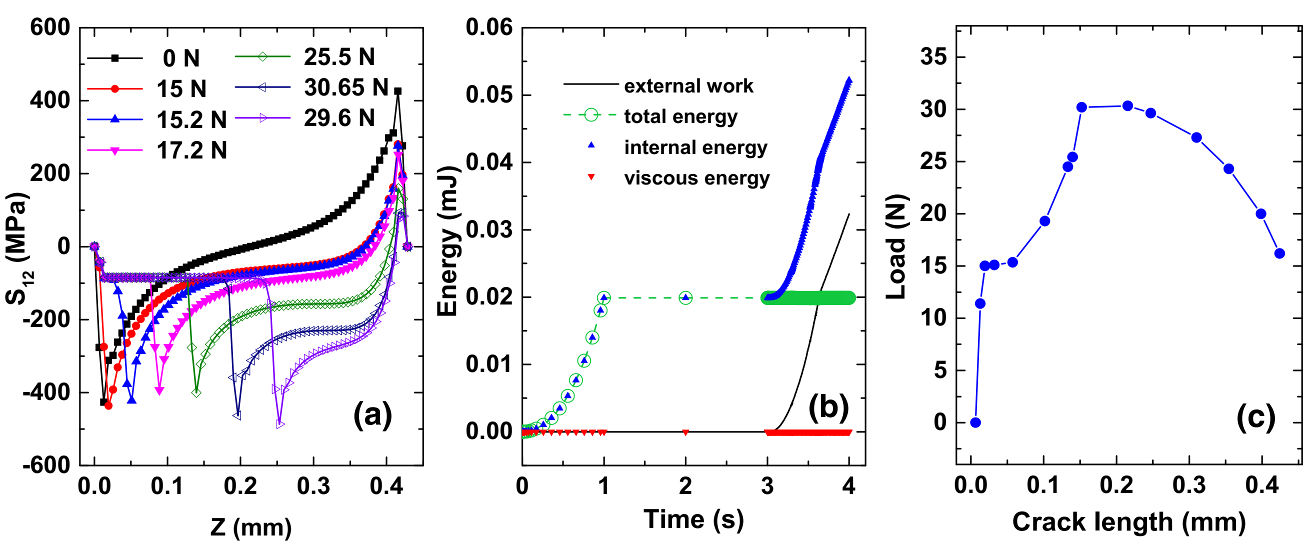

Fig. 5 (Color online) Verification simulation: **a** distribution of the shear stress, **b** changes in energy with time, **c** relationship between crack length and load

effect of the viscous coefficient introduced on the model can be ignored by comparing the internal energy and viscous energy.

Figure 5c shows the relationship between the crack length and the load. The crack does not propagate before the initial failure load, and crack propagation is based on whether sliding occurs. The load first increases quickly to ~ 15 N and then increases slowly until it reaches the maximum load (30.6 N). The crack becomes unstable when the crack tip reaches a distance equal to twice the fiber radius from the bottom of the interface and the propagation speed is higher in this stage.

The experimental and simulated averaged values of the maximum load of the fiber/matrix interfacial area and the frictional shear stress are given in Table 1. The simulated averaged maximum shear stresses and frictional shear stresses are in good agreement with the experimental results at 20, 300 and 530 °C. In addition, both the maximum and frictional shear stresses decrease with increasing test temperatures. All the compared results demonstrate that the improved cohesive element method can accurately simulate the interfacial debonding and sliding friction of SiC composites.

3 Results and discussion

3.1 Distribution of residual thermal stresses

The state of residual thermal stress is important in the fiber push-out test according to Zeng et al. [16] and Koss et al. [26], especially in metal matrix composites. The residual thermal stresses are introduced after cooling from the stress-free temperature to the testing temperature by the mismatched thermal expansion coefficients of SiC and Ti. Therefore, it is necessary to study the effects of the residual thermal stresses on the interfacial debonding and sliding friction.

The radial and axial residual thermal stresses at the center of the 430-μm-high slice in the radial direction at 20 °C are shown in Fig. 6a. The radial stress σ_{rr} is negative, because compression occurs after cooling from high to low temperature. However, it becomes positive at the matrix/average material interface because their interaction is greater than the thermal effect. In the axial direction, the stress σ_{zz} is negative in the fiber but positive in the matrix, because the thermal expansion coefficient of the fiber is smaller than that of the matrix; thus, the fiber undergoes compressive stress while the matrix endures tensile stress. The distribution of residual shear stress at the interface is given in Fig. 6b, indicating that the shear stress σ_{rz} presents an axially symmetric shape about the half-thickness of the sample, because of the axial displacement difference between the fiber and matrix at the interface. The maximum shear stress occurs at both ends of the specimen, which means that the crack is most likely to expand from both sides.

3.2 Effect of temperature

Temperature is important in the process of fiber push-out, since the introduced residual thermal stresses greatly affect the interfacial behaviors of composites. For instance, both the interfacial debonding and sliding friction are dependent on the shear stress. Figure 7a indicates the distribution of shear stress from the bottom to top along the interface under different temperatures. At 20, 300 and 530 °C, the maximum residual shear stresses are 426, 225 and 105 MPa, respectively. The residual shear stress increases with decreasing temperature. The load–displacement curves under different temperatures are given in Fig. 7b, showing that the frictional force and maximum load increases with decreasing temperature. It can be interpreted that the sliding frictional stress and maximum shear stress T_{max} increase with a decrease in temperature. Hence, the indenter force must be increased to overcome the interfacial adhesion and resistance, and the sliding frictional force increases after full debonding.

3.3 Effect of fracture strength

The critical shear strength reflects the adhesive strength between the fiber and matrix. In real applications, the cohesive strength cannot be too strong or too weak. Excessively strong cohesion easily causes fiber fracture before interfacial failure, and weak cohesion hinders the speed of load transfer from the matrix to the fiber. Figure 8 shows that the load required to cause complete interfacial failure increases with an increase in the critical shear strength, which means that the interfacial bond strength increases with the critical shear strength.

Table 1 Comparison of simulated averaged maximum and frictional shear stress with experimental values under different test temperatures

T (°C)	Averaged maximum shear stresses (MPa)			Averaged frictional shear stress (MPa)		
	Exp. 1 [16]	Exp. 2 [16]	Simulation	Exp. 1 [16]	Exp. 2 [16]	Simulation
20	160	162	160	90	77	84
300	106	112	110	21	16	20
530	47	58	55	16	0	10

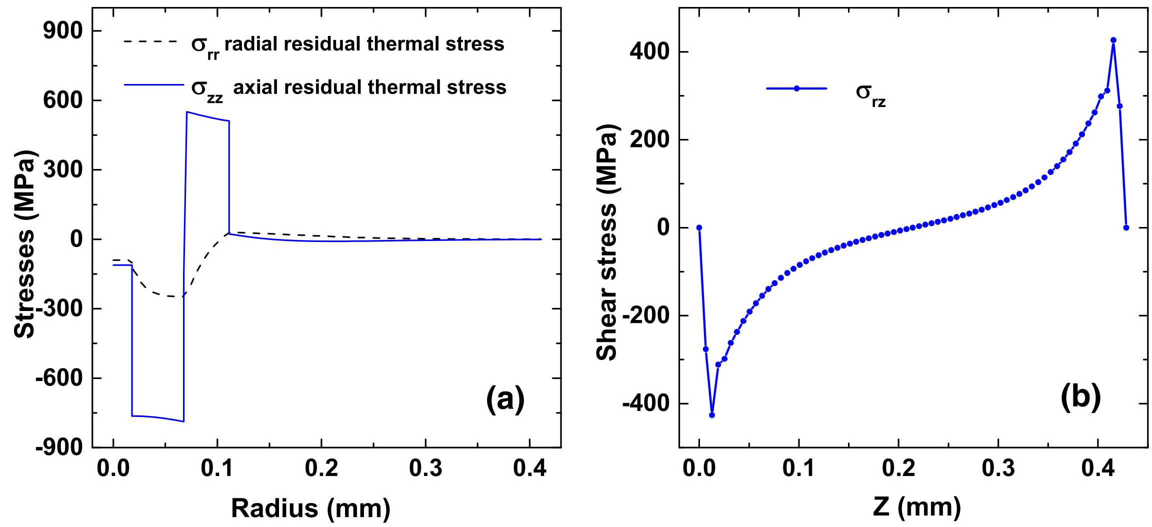

Fig. 6 (Color online) Distribution of residual thermal stresses in the middle of the slice in the radial direction (**a**) and residual shear stress from bottom to top along the interface (**b**)

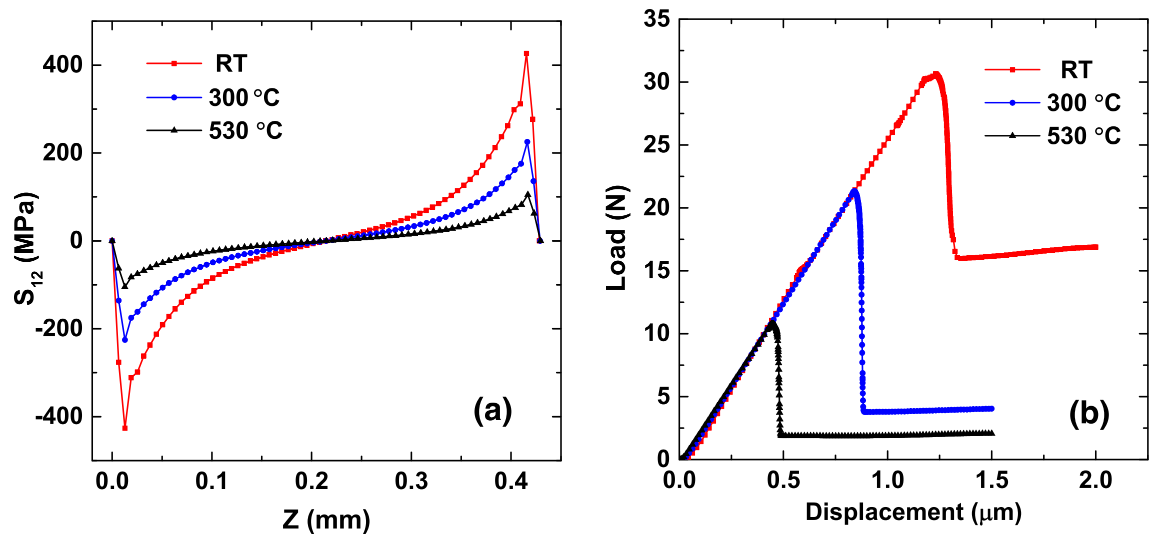

Fig. 7 (Color online) Effect of temperatures: **a** distribution of shear stress at the interface, **b** load–displacement curves under different temperatures

3.4 Effect of fiber volume fraction

The properties of a composite depend not only on its constituents but also on the volume fraction and distribution of fibers. In various processing methods, the fiber radius varies; the radius of chemical vapor deposition (CVD) of SiC fibers is approximately 100 μm. Typically, hundreds of fibers are woven together during prefabrication. The weaving methods and fiber volume fractions are critical in determining the behaviors of composites. The effect of the fiber volume fraction on the initial failure load is shown in Table 2. The initial failure load increases with increasing fiber volume fraction, meaning that a composite material with a higher fiber volume fraction has a higher bearing capacity.

3.5 Effect of interphase layer

The interphase layer is a chemical reaction layer formed during the fiber impregnation process. The interfacial layer in SiC composites comprises TiC, especially when the SiC fiber has a pure C coating [27]. In this analysis, the interphase thickness is assumed as 3 μm, 6 μm, and 9 μm, respectively. Some data [28–30] suggest that the critical shear strength and sliding frictional stress increased significantly as the interfacial reaction proceeded and that the pyrolytic carbon layer on the SiC fibers was consumed.

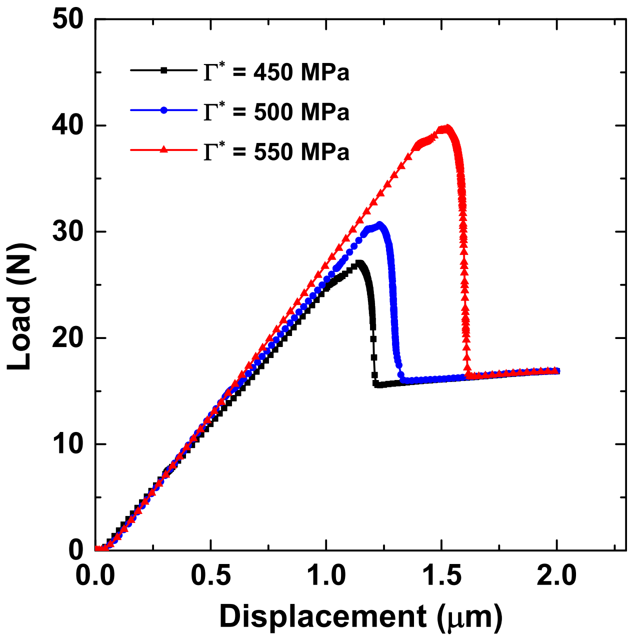

Fig. 8 (Color online) Load–displacement curves under different critical shear strengths

Table 2 Variation in the initial failure load with the fiber volume fraction

Fiber volume fraction (%)	Initial failure load (N)
30	9.93
40	13.89
50	19.61

Table 3 Variation in the initial failure load with the interfacial thickness

Thickness of interphase (μm)	Initial failure load (*N*) $\tau^* = 520$ MPa	Initial failure load (*N*) $\tau^* = 500$ MPa
3	28.00	17.24
6	44.32	32.77
9	56.81	43.83

According to Table 3, the initial failure load increases with the interfacial thickness. This is consistent with the phenomenon reported in the literature. However, the effect of the interphase is limited because the overall composite behaviors also relate to the fiber volume fraction; thus, the thickness of the interphase should not be too large.

4 Conclusion

To model sliding friction by reducing stiffness, an improved cohesive element method was presented. A finite element model based on this cohesive element was developed to evaluate the interfacial properties and analyze the effect of some geometrical and physical parameters on the behaviors of SiC fiber-reinforced Ti-matrix composites. The simulation results revealed the following:

1. According to the study of the distribution of residual shear stress, the maximum shear stress occurs at both ends of the specimen, which are the most likely locations for crack formation and propagation.
2. The temperature affects the interfacial behaviors of composites during push-out testing. Both the interfacial shear strength and the constant sliding frictional stress decrease with increasing temperature. At 20, 300 and 530 °C, the maximum residual shear stresses are 426, 225, and 105 MPa, respectively.
3. The interfacial bond strength is related to the critical shear strength, and the shear bearing capacity of the composites increases with the fiber volume fraction.
4. With the increase in interphase thickness between the matrix and the impregnated fibers, the initial failure load increases and the composite becomes more resistant to failure during the push-out test. However, the effect of the interphase is limited; this phenomenon can probably be attributed to the fiber volume fraction, which also affects the overall composite behaviors.

References

1. M.I. Idris, H. Konishi, M. Imai et al., Neutron irradiation swelling of SiC and SiCf/SiC for advanced nuclear applications. Energy Procedia. **71**, 328–336 (2015). https://doi.org/10.1016/j.egypro.2014.11.886
2. T.S. Duh, K.M. Yin, J.Y. Yan, P.C. Fang, C.W. Chen, J.J. Kai et al., Study of helium bubble formation in SiCf/PyC/??-SiC composites by dual-beam irradiation. J. Nucl. Mater. **329–333**, 518–523 (2004). https://doi.org/10.1016/j.jnucmat.2004.04.218
3. N. Chandra, H. Li, C. Shet, H. Ghonem, Some issues in the application of cohesive zone models for metal-ceramic interfaces. Int. J. Solids Struct. **39**, 2827–2855 (2002). https://doi.org/10.1016/S0020-7683(02)00149-X
4. M.N. Yuan, Y.Q. Yang, Z.J. Ma, X. Luo, B. Huang, Y. Chen, Analysis of interfacial behavior in titanium matrix composites by using the finite element method (SCS-6/Ti55). Scr. Mater. **56**, 533–536 (2007). https://doi.org/10.1016/j.scriptamat.2006.11.018
5. G.P. Tandon, N.J. Pagano, Micromechanical analysis of the fiber push-out and re-push test. Compos. Sci. Technol. **58**, 1709–1725 (1998). https://doi.org/10.1016/S0266-3538(98)00037-2
6. N. J. Pagano, Axisymetric micromechanical stress fields in composites, Local Mechanics Concepts for Composite Material Systems, 1991
7. D.K. Shetty, Shear-Lag Analysis of Fiber Push-Out (Indentation) Tests for estimating interfacial friction stress in ceramic-matrix composites., J. Am. Ceram. Soc. 71, c. 107-c. 109 (1988). https://doi.org/10.1111/j.1151-2916.1988.tb05843.x
8. C.H. Hsueh, Strength versus energy debonding criteria at fiber/matrix interfaces. Compos. Eng. **2**, 665–675 (1992). https://doi.org/10.1016/0961-9526(92)90024-Z

9. Q. Sun, X. Luo, Y.Q. Yang, B. Huang, N. Jin, W. Zhang et al., Micromechanical analysis of fiber and titanium matrix interface by shear lag method. Compos. Part B Eng. **79**, 466–475 (2015). https://doi.org/10.1016/j.compositesb.2015.05.001
10. J. Dinter, P.W.M. Peters, J. Hemptenmacher, Finite element modelling of the push-out test for SiC fibre-reinforced titanium alloys. Compos. Part A Appl. Sci. Manuf. **27**, 749–753 (1996). https://doi.org/10.1016/1359-835X(96)00025-5
11. C.R. Ananth, N. Chandra, Numerical modeling of fiber push-out test in metallic and intermetallic matrix composites-mechanics of the failure process. J. Compos. Mater. (1995). https://doi.org/10.1177/002199839502901105
12. K. Honda, Y. Kagawa, Analysis of shear stress distribution in pushout process of fiber-reinforced ceramics. Acta Metall. Mater. **43**, 1477–1487 (1995). https://doi.org/10.1016/0956-7151(94)00355-L
13. M.N. Yuan, Y.Q. Yang, B. Huang et al., Evaluation of interface fracture toughness in SiC fiber reinforced titanium matrix composite. Trans. Nonferrous Met. Soc. China **18**, 925–929 (2008). https://doi.org/10.1016/S1003-6326(08)60160-0
14. A.F. Kalton, S.J. Howard, J. Janczak-Rusch, T.W. Clyne, Measurement of interfacial fracture energy by single fibre push-out testing and its application to the titanium–silicon carbide system. Acta Mater. **46**, 3175–3189 (1998). https://doi.org/10.1016/S1359-6454(98)00009-3
15. Y.F. Liu, Y. Kagawa, Analysis of debonding and frictional sliding in fiber-reinforced brittle matrix composites: basic problems. Mater. Sci. Eng. A **212**, 75–86 (1996). https://doi.org/10.1016/0921-5093(96)10196-9
16. W.D. Zeng, P.W.M. Peters, Y. Tanaka, Interfacial bond strength and fracture energy at room and elevated temperature in titanium matrix composites (SCS-6/Timetal 834). Compos. Part A Appl. Sci. Manuf. **33**, 1159–1170 (2002). https://doi.org/10.1016/S1359-835X(02)00089-1
17. P.H. Geubelle, J.S. Baylor, Impact-induced delamination of composites: a 2D simulation. Compos. Part B Eng. **29**, 589–602 (1998). https://doi.org/10.1016/S1359-8368(98)00013-4
18. G. Lin, P.H. Geubelle, N.R. Sottos, Simulation of fiber debonding with friction in a model composite pushout test. Int. J. Solids Struct. **38**, 8547–8562 (2001). https://doi.org/10.1016/S0020-7683(01)00085-3
19. J.H. You, W. Lutz, H. Gerger et al., Fiber push-out study of a copper matrix composite with an engineered interface: experiments and cohesive element simulation. Int. J. Solids Struct. **46**, 4277–4286 (2009). https://doi.org/10.1016/j.ijsolstr.2009.08.021
20. H. Chen, W. Hu, Y. Zhong, G. Gottstein, Finite element analysis of single-fiber push-out tests of continuous Al_2O_3 fiber-reinforced NiAl composites. Mater. Sci. Eng. A **460–461**, 624–632 (2007). https://doi.org/10.1016/j.msea.2007.01.087
21. H. Ho, L.T. Drzal, Evaluation of interfacial mechanical properties of fiber reinforced composites using the microindentation method. Compos. Part A Appl. Sci. Manuf. **27**, 961–971 (1996). https://doi.org/10.1016/1359-835X(96)84802-0
22. S. Mukherjee, C.R. Ananth, N. Chandra, Effect of residual stresses on the interfacial fracture behavior of metal-matrix composites. Compos. Sci. Technol. **57**, 1501–1512 (1997). https://doi.org/10.1016/S0266-3538(97)00081-X
23. M.N. Yuan, Y.Q. Yang, H.J. Luo, Evaluation of interfacial properties in SiC fiber reinforced titanium matrix composites using an improved finite element model. Mater. Charact. **59**, 1684–1689 (2008). https://doi.org/10.1016/j.matchar.2008.03.010
24. N. Chandra, Evaluation of interfacial fracture toughness using cohesive zone model. Compos. Part A. Appl. Sci. Manuf. **33**(10), 1433–1447 (2002). https://doi.org/10.1016/S1359-835X(02)00173-2
25. Dassault Systèmes, ABAQUS Version 6.10 HTML Documentation, 2010
26. D.A. Koss, M.N. Kallas, J.R. Hellmann, Mechanics of interfacial failure during thin-slice fiber pushout tests. MRS Proc. (1993). https://doi.org/10.1557/proc-273-303
27. X. Yanfang, S. Tiexiong, Y. Meini, Study of interfacial stress distribution in SiC fiber reinforced titanium matrix composites on transverse tensile tests. J. Mater. Eng. Perform. **21**, 2446–2450 (2012). https://doi.org/10.1007/s11665-011-0094-y
28. J.I. Eldridge, P.K. Brindley, Investigation of interfacial shear strength in a SiC fibre/Ti-24Al-11Nb composite by a fibre push-out technique. J. Mater. Sci. Lett. **8**, 1451–1454 (1989). https://doi.org/10.1007/BF00720221
29. C.J. Yang, S.M. Jeng, J.M. Yang, Interfacial properties measurement for SiC fiber-reinforced titanium alloy composites. Scr. Metall. Mater. **24**, 469–474 (1990). https://doi.org/10.1016/0956-716X(90)90184-I
30. M.C. Watson, T.W. Clyne, The use of single fibre pushout testing to explore interfacial mechanics in SiC monofilament-reinforced Ti-I. A photoelastic study of the test. Acta Metall. Mater. **40**, 131–139 (1992). https://doi.org/10.1016/0956-7151(92)90206-T